Original Article

MOLECULAR METABOLISM

Sestrin2 maintains hepatic immune homeostasis and redox balance partially via inhibiting RIPK3-mediated necroptosis in metabolic dysfunction-associated steatohepatitis

Jian-Bin Zhang[1], **Qian-Ren Zhang**[1], **Qian Jin**, **Jing Yang**, **Shuang-Zhe Lin**, **Jian-Gao Fan***

ABSTRACT

Background & aims: Necroptosis, a novel type of programmed cell death, is intricately associated with inflammatory response. Currently, most studies focus on the activation of necroptosis, while the mechanisms underlying the negative regulation of necroptosis remain poorly understood.
Methods: The effects of sestrin2 (SESN2) overexpression or knockdown on the regulation of necroptosis were assessed in the TNFα/Smac-mimetic/Z-VAD-FMK (T/S/Z)-induced necroptosis model and palmitic acid (PA)-induced lipotoxicity model. Western-blot, co-Immunoprecipitation, Glutathione S-transferase pull-down, and confocal assays were employed to explore the regulatory mechanisms including protein—protein interactions and post-translational modification. Furthermore, we used GSK'872, a specific inhibitor of receptor-interacting serine/threonine-protein kinase (RIPK) 3, to evaluate the relationship between SESN2-related alterations and RIPK3-mediated necroptosis in T/S/Z-induced necroptosis model, PA-induced lipotoxicity model, and high-fat high-cholesterol diet (HFHCD)-induced non-alcoholic steatohepatitis model.
Results: Our findings revealed that SESN2 was upregulated under conditions that induce necroptosis and functioned as a negative regulator of necroptosis. High levels of SESN2 could equipped hepatocytes with the ability to defend against necroptotic inflammation and oxidative stress. Mechanistically, SESN2 interacted with RIPK3 and tuned down necroptosis by inhibiting the phosphorylation of RIPK3, promoting the ubiquitination of RIPK3, and preventing the formation of the RIPK1/RIPK3 necrosome. The depletion of SESN2 resulted in excessive necroptosis, accompanied by increased fat accumulation, inflammation, and oxidative stress in the experimental steatohepatitis model. Blocking necroptosis by GSK'872 reduced the liberation of pro-inflammatory cytokines and reactive oxygen species generation, but not hepatocyte fat deposition, in both PA-treated SESN2 knockout cells and HFHCD-fed SESN2 knockout mice, suggesting that the activation of RIPK3-mediated necroptosis may partially account for the hyperinflammation and excessive oxidative stress induced by SESN2 deficiency.
Conclusion: Our results suggested that SESN2 inhibited RIPK3-mediated necroptosis; this regulation is an important for the immune homeostasis and the redox balance in the liver.

Keywords SESN2; Necroptosis; RIPK3; MASH; Inflammation; Oxidative stress

1. INTRODUCTION

Non-alcoholic fatty liver disease (NAFLD) represents a spectrum of liver damage ranging from nonalcoholic fatty liver (NAFL) to nonalcoholic steatohepatitis (NASH), and then cirrhosis and hepatocellular carcinoma (HCC) [1,2]. However, some experts argue that the terms NAFLD and NASH fail to elucidate the etiology of the disease, thereby potentially overlooking the significant contributions of cardiometabolic risk factors, insulin resistance, visceral adiposity, and adipose tissue dysfunction in patients [3]. Therefore, the implementation of a novel terminology has occurred, whereby individuals presenting with steatosis or steatohepatitis, along with the presence of at least one cardiometabolic risk factor, are now classified as subjects affected by metabolic dysfunction-associated steatotic liver disease (MASLD) or metabolic dysfunction-associated steatohepatitis (MASH) [4]. Although, MASLD/MASH has emerged as the most prevalent chronic liver condition worldwide [5], the precise mechanisms driving MASH remain incompletely understood.

The balance between cell survival and cell death is essential for the maintenance of cell, tissue, and organism homeostasis [6]. Traditionally, cell death has been classified into apoptosis or necrosis [7,8]. However, recent research has unveiled a new programmed cell death, termed necroptosis, which overturned this simple dichotomy and revealed a more intricate and intertwined landscape of cell death. Necroptosis is a form of regulated cell death in a manner similar to apoptosis, but typically exhibits similar morphological characteristics as necrosis [9].

Department of Gastroenterology, Xin Hua Hospital affiliated to Shanghai Jiao Tong University School of Medicine, Shanghai 200092, China

[1] Equal contributors.

*Corresponding author. E-mail: fanjiangao@xinhuamed.com.cn (J.-G. Fan).

Received September 25, 2023 • Revision received December 22, 2023 • Accepted December 23, 2023 • Available online 30 December 2023

https://doi.org/10.1016/j.molmet.2023.101865

Abbreviations

ALT	alanine aminotransferase
ALP	alkaline phosphatase
AST	aspartate aminotransferase
CCK8	cell counting kit-8
COL1A1	collagen type I alpha 1 chain
DAMPs	danger-associated molecular patterns
ER	endoplasmic reticulum
FBS	fetal bovine serum
PI	propidium iodide
T/S/Z	TNF-α/SM-164/Z-VAD-FMK
GST	Glutathione S-transferase
GAPDH	glyceraldehyde 3-phosphate dehydrogenase
GSH	glutathione
HFHCD	high-fat high-cholesterol diet
HE	hematoxylin and eosin
HSC	hepatic stellate cells
MASH	metabolic dysfunction-associated steatohepatitis
MASLD	metabolic dysfunction-associated steatotic liver disease
MDA	malondialdehyde
MLKL	mixed lineage kinase domain-like protein
NAC	N-acetyl-L-cysteine
NAFLD	non-alcoholic fatty liver diseases
NASH	non-alcoholic steatohepatitis
ANOVA	one-way analysis of variance
PA	palmitic acid
ROS	reactive oxygen species
RIPK1/3	receptor-interacting protein kinase 1/3
SESN2	sestrin2
SESN2 KO	SESN2 knockout
SESN2 WT	SESN2 wild-type
SD	standard deviation
TBST	tris-buffered saline containing 0.1 % Tween-20
TC	total cholesterol
TG	triglyceride
TNFR	TNF receptor
TNF-R1	TNF receptor 1
TUBEs	Tandem Ubiquitin Binding Entities

The molecular mechanism of necroptosis involves two Receptor-Interacting Protein Kinase (RIPK) 1/3 and the mixed lineage kinase domain-like protein (MLKL). Phosphorylated RIPK3, as the primary initiator of necroptosis, interacts with RIPK1 to form the necrosome, which subsequently phosphorylates the necroptosis executioner MLKL [10—12]. The phosphorylated MLKL is then oligomerized, translocated to plasma membrane the plasma membrane to compromise membrane integrity and execute necroptosis [10,11]. This leads to the release of danger-associated molecular patterns (DAMPs) and triggers a robust immune response, ultimately resulting in the development of inflammatory diseases, such as MASH [13—15]. Despite extensive research on necroptosis, the mechanisms underlying the negative regulation of necroptosis were still insufficient. Therefore, investigating the negative regulation of necroptosis and its impact on immune response modulation is of paramount significance.

Sestrin2 (SESN2) is a highly evolutionarily conserved stress-inducible protein that can be up-regulated in response to multiple stimuli [16]. Accumulative evidence supported the significant role of SESN2 in monitoring and maintaining hepatocyte survival and liver homeostasis [17,18]. Moreover, SESN2 was identified as the only subtype among the sestrins family that could be induced by saturated fatty acids in HepG2 cells [19]. However, how SESN2 functions as a 'brake' in MASH progression, and especially the negative role of SESN2 in inflammation, remain largely unclear. Notably, recent research suggested that the emission of DAMPs, including inflammatory cytokines, DNA fragments, and damaged organelles (e.g., mitochondria and endoplasmic reticulum (ER)), from necroptotic cells can serve as upstream signaling molecules that effectively activate the expression of SESN2 [13,14,16,17,20]. This suggested to us that there might exist undiscovered connections between SESN2 and necroptosis, and that certain functions of SESN2 in MASH may be mediated by regulating necroptosis.

2. MATERIALS AND METHODS

2.1. Cell culture and reagents

The HepG2 cell lines were purchased from American Type Culture Collection. The cells were cultured in DMEM (Gibco, USA) supplemented with 10 % fetal bovine serum (FBS, Biological Industries, Israel) and incubated in a humidified atmosphere containing 5 % CO2 at 37 °C. The chemical reagents used in this study are listed in Supplementary Table 1.

2.2. Animal experiments

All animal handling and experimental procedures were approved by the Animal Care and Use Committee of Xinhua Hospital, affiliated with Shanghai Jiao Tong University School of Medicine. SESN2 knockout (SESN2 KO) C57BL/6 mice were kindly provided by Dr. Wenning Xu (Department of Clinic of Spine Center, Xinhua Hospital, Shanghai Jiaotong University School of Medicine, Shanghai, China.) and described previously [21]. Mice were housed in a specific pathogen-free barrier environment facility with a 12-hour light/dark cycle throughout the study. Eight-week-old male SESN2 wild-type (SESN2 WT) and SESN2 KO mice were fed a standard chow diet or a high-fat high-cholesterol diet (HFHCD, fat 33 kcal%, carbohydrates 50 kcal%, protein 17 kcal%, and 2 % cholesterol; TrophicDiet, Nantong, China) for 16w [22,23]. At the end of 8 weeks, the mice fed with HFHCD were administered intraperitoneally with either the vehicle control or GSK'872 at a dose of 1.0 mg/kg twice weekly for the next 8 weeks. Upon completion of the experiments, the mice were fasted for 12 h and weighed, followed by collection of blood samples before euthanasia. All the animals were humanely euthanized by intraperitoneal injection of pentobarbital sodium.

2.3. Histological analysis

The liver tissues were fixed in formalin and embedded in paraffin wax, which was then cut into 6 μm sections and mounted on glass slides for hematoxylin and eosin (HE) staining according to standard procedures as described previously [24]. Immunohistochemical staining was conducted on paraffin-embedded liver sections using F4/80 or LyG6 antibodies to evaluate the infiltration of hepatic macrophages and neutrophils, respectively, according to the previously described protocols [25,26].

2.4. Western blot

The Western blot analysis was performed as previously described [27]. Briefly, the mouse liver tissues or cultured cells were evenly homogenized and lysed at 4 °C in lysis buffer containing protease inhibitors and phosphatase inhibitor cocktail. The lysates were then

centrifuged at 16,000 rpm for 15 min at 4 °C and the resulting supernatant was used for Western blot analysis. The protein concentration was measured using a BCA protein assay kit. For Western blotting, 30—50 μg of protein was separated by 8%—12 % SDS-PAGE and then transferred onto polyvinylidene fluoride membranes using transfer buffer (25 mM Tris-base, 190 mM glycine, and 20 % methanol) at 300 mA. The membranes were incubated with 5 % non-fat milk in Tris-buffered saline containing 0.1 % Tween-20 (TBST) at room temperature for 2 h to block non-specific binding, and then probed with specific primary antibodies overnight at 4 °C. Afterward, the membranes were incubated with HRP-conjugated secondary antibodies to enable the detection of the target proteins. The signals were visualized using the Immobilon Western Chemiluminescent HRP substrate and captured using a Bio-Rad ChemiDoc XRS + system. Bio-Rad Image Lab Version 2.0.1 software was employed for signal quantification. The antibodies used in this study are listed in Supplementary Table 2.

2.5. Quantitative real-time PCR

The total RNA was extracted from mouse liver tissues and HepG2 cells using the Trizol reagent. Reverse transcription was carried out using the PrimeScript RT Master Mix cDNA Synthesis Kit to obtain the first strand cDNA. Real-time PCR was performed on a ViiA7 RT-PCR system (Applied Biosystems, Foster City, CA, USA) with SYBR Premix following the manufacturer's instructions. The relative expression of the target genes was determined using the 2-ΔΔCt method and normalized to Glyceraldehyde 3-phosphate dehydrogenase (GAPDH). The primer sequences used are listed in Supplementary Table 3.

2.6. Co-immunoprecipitation

The HepG2 cells were evenly homogenized and lysed at 4 °C in cell lysis buffer supplemented with a complete protease inhibitor cocktail. The lysates were then centrifuged at 16,000 rpm for 10 min at 4 °C. A small portion of the resulting supernatant was analyzed by Western blot, while the remaining supernatant was incubated with the specific primary antibodies overnight with slow shaking at 4 °C. T10μl of protein A agarose beads were washed 3 times with an appropriate amount of lysis buffer, and centrifuged at 3,000 rpm for 2 min each time. The next day, 10 μl of protein A agarose beads were washed 3 times with 1 ml of lysis buffer, and centrifuged at 3,000 rpm for 2 min each time. Then, the cell supernatant that had been incubated with the antibody overnight were added with washed 10 μl protein A agarose beads and incubated with slow shaking (4 °C, 2 h) to couple the antibody to the protein A agarose beads. Following immunoprecipitation, the lysate was centrifuged for 3 min at 3,000 rpm at 4 °C. The supernatant was then gently removed, and the agarose beads were washed with 1 ml of lysis buffer for 3—4 times. Afterward, 20 μl of 2 × SDS loading buffer was added and boiled for 5—10 min. The resulting samples were subsequently utilized for Western blot analysis.

2.7. Glutathione S-transferase (GST) pull-down

Detailed methods were performed as described [28]. Briefly, to conduct GST pull-down assays, the plasmids encoding for SESN2-GST or RIPK3-His were introduced into *Escherichia coli* BL21 strain. The recombinant protein expression was induced by treating the cells with 0.2 mM isopropyl-b-D-thiogalactoside at 16 °C overnight. The immobilized and purified GST fusion proteins were then incubated with the purified RIPK3-His protein. The bound proteins were subsequently subjected to washing steps and analyzed by western blot using anti-His antibody. The recombinant DNA used in this study are listed in Supplementary Table 4.

2.8. Immunofluorescence confocal microscopy

HEK293T or HepG2 cells were co-transfected with the Flag-tagged SESN2 and Myc-tagged RIPK3 plasmids. Immunofluorescence and confocal microscopy were performed as described previously [29].

2.9. Tandem ubiquitin binding entities (TUBEs) pull down

The TUBEs pull down assay was performed using TUBE2-Agarose beads (Life Sensors) following the manufacturer's instructions.

2.10. Statistical analysis

The data are presented as mean ± standard deviation (SD). Statistical analysis was performed using GraphPad Prism 7 software. One-way analysis of variance (ANOVA) was used to compare the means among multiple groups, followed by Tukey's post hoc test for multiple comparisons. The significance level was set at $P < 0.05$. Additional methods are provided in Supplementary methods.

3. RESULT

3.1. The deletion of SESN2 could exacerbate TNF-α/SM-164/Z-VAD-FMK (T/S/Z)-induced necroptosis, potentially serving as a mechanism through which SESN2 KO aggravated inflammation and oxidative stress

To investigate the potential physiological functions of SESN2 in T/S/Z-induced necroptosis, we employed CRISPR-Cas9 technology with independent single guide RNAs (Supplementary Table 5) to generate SESN2 KO HepG2 cells (Supplementary Fig. 1A). In this study, we found that knockout of SESN2 aggravated T/S/Z-induced cell death (Figure 1A—C). Moreover, following stimulation with T/S/Z, the phosphorylation levels of necroptosis kinases (e.g., RIPK1, RIPK3, and MLKL) exhibited a significant time-dependent increase in SESN2 KO HepG2 cells compared to SESN2 WT HepG2 cells (Figure 1D). Conversely, no elevation in cleaved caspase-3 levels was detected between the two groups, suggesting that the augmented cell death observed in SESN2 KO HepG2 cells after T/S/Z treatment primarily occurred through necroptosis rather than apoptosis (Supplementary Fig. 1B). The cumulative evidence suggested that necroptosis is closely linked to inflammation and oxidative stress [13,14,20] [[,]] [30,31]. Similarly, our present study revealed that T/S/Z treatment resulted in the induction of inflammatory markers such as IL-1β and TNF-α, as well as oxidative stress indicators including reactive oxygen species (ROS) and lipid peroxidation (Figure 1E—H, Supplementary Figs. 1C—D). In addition, the exacerbation of these effects was observed in the context of SESN2 deletion (Figure 1E—H, Supplementary Figs. 1C—D).

Therefore, to further ascertain the potential association between the exacerbated inflammation and oxidative stress after knocking out SESN2 and the activated necroptosis, we employed the necroptosis inhibitor, GSK'872. The findings of our study indicated that the treatment of GSK'872 resulted in significantly decreased levels of IL-1β and ROS in T/S/Z-treated SESN2 WT and KO HepG2 cells (Figure 1J—K). However, it is important to note that the effect mediated by GSK-872 was incomplete, suggesting that SESN2 knockout-related changes were not solely due to the activation of necroptosis (Figure 1J—K). There could potentially exist additional mechanisms, such as TNF receptor (TNFR) signaling, that contribute to the impact of SESN2 knockout. As expected, we found SESN2 knockout significantly increased the expression of TNF -receptor 1 (TNF-R1) and p-ERK (Figure 1I). Interestingly, GSK'872 exhibited the ability to reduce TNF-R1 and p-ERK expression in both SESN2 WT and KO cells (Figure 1I), implying that the activation of necroptosis and TNFR1 signaling are not

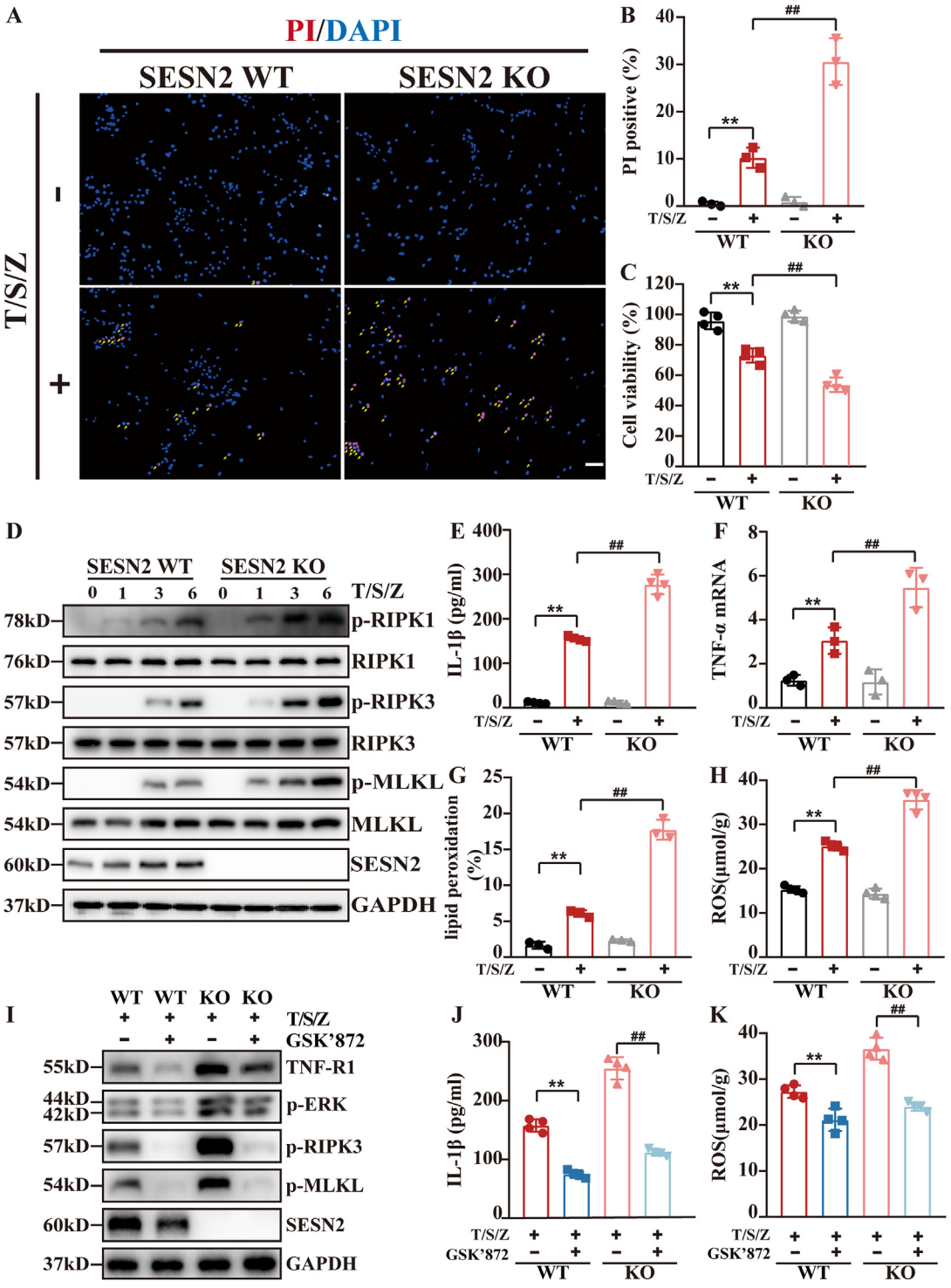

Figure 1: The deletion of sestrin2 (SESN2) aggravated inflammation and oxidative stress partially via necroptosis activation. (A, B) SESN2 wild-type (SESN2 WT) and SESN2 knockout (SESN2 KO) HepG2 cells were treated with necrotic stimulation (T/S/Z; human TNF-α (30 ng/mL), SM-164 (1 μM), and zVAD (20 μM)) for 6h. Cells were then stained with 4′,6-diamidino-2-phenylindole (DAPI) and propidium iodide (PI) for nuclei. Representative images and quantification of PI-positive cells were shown; yellow arrows point to necroptosis. Scale bar = 100 μm. (C) The viability of SESN2 WT and KO HepG2 cells was measured by using the cell counting kit-8 (CCK8) assay. (D) Western blot analysis of receptor-interacting protein kinase (RIPK)1, p-RIPK1, RIPK3, p-RIPK3, mixed lineage kinase domain-like protein (MLKL), p-MLKL and SESN2 over time in SESN2 WT and SESN2 KO HepG2 cells. (E, J) The level of IL-1β in T/S/Z-treated SESN2 WT and KO HepG2 cells was measured in cell culture supernatant by a commercial ELISA kit. (F) Relative mRNA level of TNF-α in SESN2 WT and KO HepG2 cells. (G) The lipid peroxidation assessment was determined by C11-BODIPY 581/591 and flow cytometry in SESN2 WT and KO HepG2 cells. The percentage of lipid peroxidation in each group. (H, K) The contents of reactive oxygen species (ROS) in SESN2 WT and KO HepG2 cells were detected with *in vitro* ROS/reactive nitrogen species assay kit. (I) Western blot analysis of TNF-receptor 1 (TNF-R1), p-ERK, p-RIPK3, p-MLKL, and SESN2 over time in SESN2 WT and SESN2 KO HepG2 cells with or without GSK'872. All the data are expressed as the mean ± SD (n = 3–4). *p < 0.05, **p < 0.01 for SESN2 WT vs SESN2 WT-T/S/Z, and SESN2 WT-T/S/Z vs SESN2 WT-T/S/Z + GSK'872; #p < 0.05, ##p < 0.01 for SESN2 WT-T/S/Z vs SESN2 KO-T/S/Z, and SESN2 KO-T/S/Z vs SESN2 KO-T/S/Z + GSK'872.

entirely distinct mechanisms, but rather exhibit a certain degree of intercommunication. Collectively, the deletion of SESN2 could exacerbate T/S/Z-induced necroptosis, potentially serving as a mechanism through which SESN2 modulates inflammation and oxidative stress.

3.2. Overexpression of SESN2 exerted anti-inflammatory and antioxidant effects partially by inhibiting T/S/Z-induced necroptosis activation

To further validate the involvement of SESN2 in the necroptosis model, we conducted SESN2 overexpression experiments in T/S/Z-treated HepG2 cells using Flag-SESN2 plasmid. We found that the survival of HepG2 cells treated with T/S/Z was significantly prolonged by SESN2 overexpression (Figure 2A). Consistently, overexpression of SESN2 led to reduced phosphorylation levels of RIPK1, RIPK3, and MLKL following T/S/Z treatment (Figure 2B). We further studied whether SESN2 modulates inflammation and oxidative stress through regulating the activation of necroptosis. Our findings demonstrated that SESN2 overexpression significantly reduced inflammatory markers such as IL-1β and TNF-α, as well as oxidative stress indicators including ROS and lipid peroxidation (Figure 2C–F; Supplementary Figs. 2A–B). More importantly, we found that GSK'872 treatment reduced the production of IL-1β in T/S/Z-treated cells to a level comparable that achieved by SESN2 overexpression (Figure 2G), but GSK'872 treatment did not further reduce the level of IL-1β in SESN2 overexpression HepG2 cells (Figure 2G), suggesting that SESN2 may ameliorated inflammation largely through regulating the activation of necroptosis in T/S/Z-induced necroptosis model. Interestingly, we found that GSK'872 exhibited a marginally inferior impact on the reduction of ROS compared to the overexpression of SESN2 (Figure 2H); similarly, GSK'872 treatment did not further reduce the levels of ROS in SESN2 overexpression HepG2 cells (Figure 2H). Collectively, these results provide compelling evidence supporting the essential role of SESN2 in restraining necroptosis and equipped liver cells with the ability to defend against inflammation and oxidative stress in T/S/Z-induced cell necroptosis model.

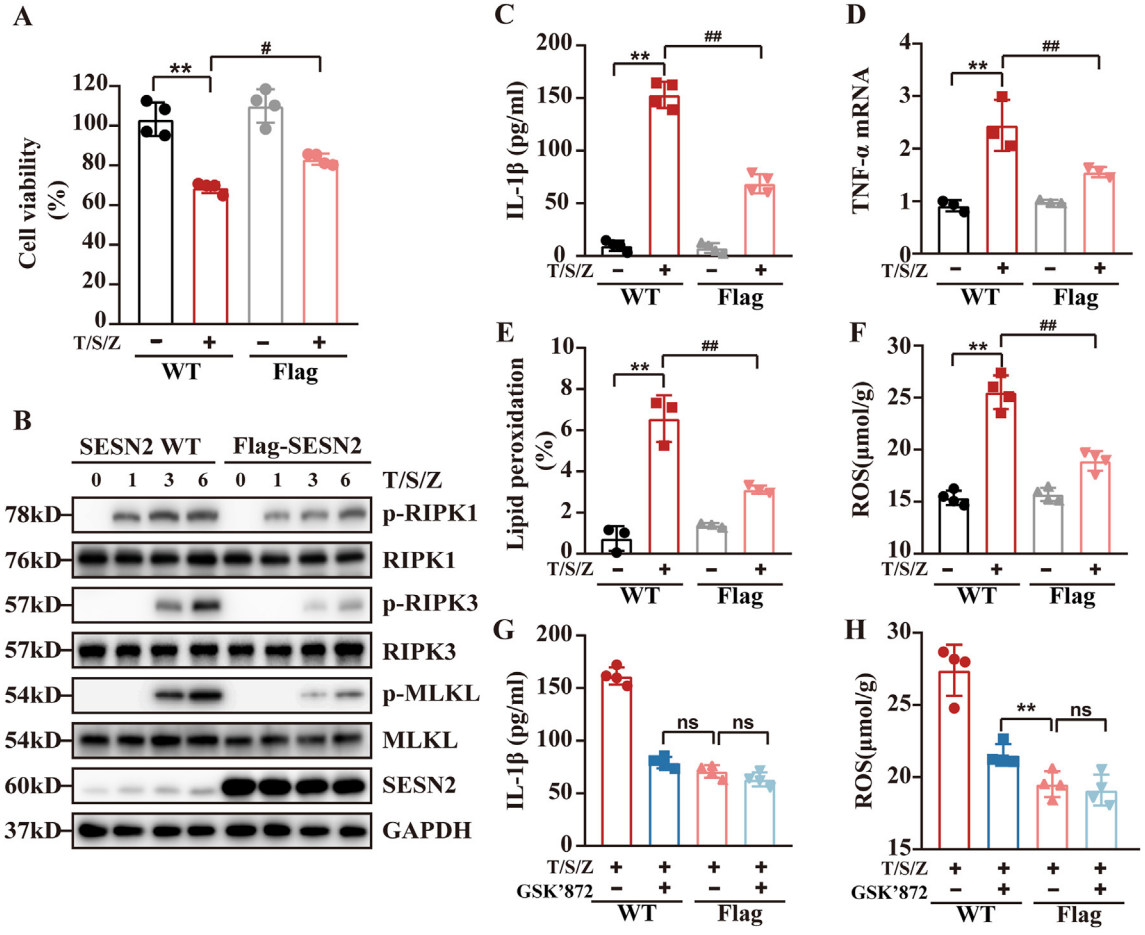

Figure 2: Overexpression of SESN2 protected against T/S/Z-induced inflammation and oxidative stress partially by inhibiting necroptosis. (A) The viability of SESN2 WT and Flag-SESN2 HepG2 cells exposed to T/S/Z for 6h was measured by using CCK8 assay. (B) Western blot analysis of p-RIPK1, RIPK1, p-RIPK3, RIPK3, p-MLKL, MLKL and SESN2 over time in SESN2 WT and Flag-SESN2 HepG2 cells. (C, G) The level of IL-1β in T/S/Z-treated SESN2 WT and Flag-SESN2 HepG2 cells was measured in cell culture supernatant by a commercial ELISA kit. (D) Relative mRNA level of TNF-α was assessed in SESN2 WT and Flag-SESN2 HepG2 cells treated with T/S/Z for 6h. (E) The lipid peroxidation assessment was determined by C11-BODIPY 581/591 and flow cytometry in SESN2 WT and Flag-SESN2 HepG2 cells. The percentage of lipid peroxidation in each group. (F, H) The contents of ROS in SESN2 WT and Flag-SESN2 HepG2 cells were detected with *in vitro* ROS/reactive nitrogen species assay kit. All the data are expressed as the mean ± SD (n = 3–4). *p < 0.05, **p < 0.01 for SESN2 WT vs SESN2 WT-T/S/Z, and SESN2 WT-T/S/Z + GSK'872 vs Flag-SESN2-T/S/Z; #p < 0.05, ##p < 0.01 for SESN2 WT-T/S/Z vs Flag-SESN2-T/S/Z.

3.3. SESN2 modulated RIPK3-mediated necroptosis by suppressing RIPK3 phosphorylation, enhancing its ubiquitination, and preventing the formation of the RIPK1/RIPK3 necrosome

To investigate the potential interaction between SESN2 and critical necroptosis kinases, such as RIPK1, RIPK3, and MLKL, we conducted co-immunoprecipitation assays. Our results revealed that under normal culture conditions, endogenous SESN2 co-immunoprecipitated with RIPK3 but not with RIPK1 or MLKL (Figure 3A—B). Moreover, following T/S/Z treatment, the interaction between SESN2 and RIPK3 was significantly enhanced (Figure 3A—B). To further explore the direct binding between SESN2 and RIPK3, we performed *in vitro* GST pull-down experiments. As depicted in Figure 3C, GST-SESN2, but not GST alone, exhibited interaction with His-RIPK3 protein. Additionally, immunofluorescence confocal microscopy assays demonstrated colocalization of SESN2 and RIPK3 in HEK293T and HepG2 cells (Figure 3D, Supplementary Fig. 3A). Furthermore, utilizing the AlphaFold2 structure prediction tool, we analyzed the structural aspects of the SESN2-RIPK3 interaction, revealing a well-chimeric surface between the two proteins (Figure 3E, Supplementary Fig. 3B). The interaction interface amino acids were further analyzed using the PLIP web server [32] and LigPlot [33] (Figure 3E, Supplementary Fig. 3B). These findings provided solid evidence that SESN2 could directly bind to RIPK3 both *in vivo* and *in vitro*.

To elucidate how SESN2 regulates RIPK3-mediated necroptosis, we investigated the post-translational modifications of RIPK3, which have been identified as crucial for the activation of necroptosis [34]. In addition to confirming the effects of SESN2 on modulating RIPK3 phosphorylation, we observed that SESN2 knockout significantly decreased the ubiquitination of RIPK3 (Figure 3F). Conversely, SESN2 overexpression efficiently increased RIPK3 ubiquitination under necroptotic conditions (Figure 3G). Furthermore, we employed Flag-SESN2 overexpression plasmid to express SESN2 in SESN2 KO HepG2 cells. The induction of SESN2 resulted in a reduced formation of the necrosome (RIPK1-RIPK3) (Figure 3H). These findings suggested that SESN2 modulated RIPK3-mediated necroptosis by suppressing RIPK3 phosphorylation, enhancing its ubiquitination, and preventing the formation of the RIPK1/RIPK3 necrosome.

3.4. SESN2 protected against palmitic acid (PA)-induced inflammation and oxidative stress partially through the inhibition of necroptosis activation

We identified the cell sources in which SESN2 levels were upregulated under lipotoxic stimulation. Primary hepatocytes, Kupffer cells (F4/80+CD11b+), and hepatic stellate cells were isolated from SESN2 WT mouse livers using gradient centrifugation or FACS sorting. As shown in Supplementary Fig. 4A, after 24 h of stimulation with 250 μM PA, SESN2 expression was upregulated in hepatocytes and Kupffer cells, but not in hepatic stellate cells (HSC). Notably, SESN2 expression increased more than 5-fold in hepatocytes under PA stimulation, while it increased only over 2-fold in Kupffer cells (Supplementary Fig. 4A). Moreover, hepatocytes, the main cell type in the liver, comprise 70 % of the total cell number in the liver, which are much higher than the other hepatic nonparenchymal cells (e.g., Kupffer cells, HSC). Therefore, we speculated that hepatocyte might serve as the primary origin of SESN2 during MASLD development.

Next, we explored the relationship between SESN2 and necroptosis in PA-induced lipotoxicity model. It was observed that the PA stimulation resulted in a noteworthy time-dependent increase in the expression of SESN2 in WT HepG2 cells (Figure 4A). Moreover, we found that the knockout of SESN2 exacerbated cell death induced by PA stimulation (Figure 4B and Supplementary Figs. 4B—D). Notably, unlike T/S/Z treatment, which selectively induces necroptosis [35—37], PA has been shown to elicit various forms of cell death, including apoptosis, ferroptosis, and necroptosis [38,39]. Therefore, it is imperative to ascertain whether the knockout of SESN2 could exacerbate cell death induced by PA through the activation of necroptosis. Here, we observed an augmented phosphorylation of necroptotic kinases (RIPK1/RIPK3/MLKL) in SESN2 KO HepG2 cells compared to SESN2 WT HepG2 cells, indicating the involvement of necroptosis in the heightened cell death induced by SESN2 knockout (Figure 4A). Moreover, we found that knockout of SESN2 resulted in reduced levels of ubiquitinated RIPK3 in PA-treated HepG2 cells (Supplementary Fig. 4E). Furthermore, we discovered that the administration of GSK'872 significantly mitigated PA-induced cell death in SESN2 knockout HepG2 cells (Figure 4B). Finally, we examined the impact of the necroptosis inhibitor GSK'872, the ferroptosis inhibitor ferrostatin-1, the apoptosis inhibitor Z-VAD-fmk, and the ROS scavenger N-acetyl-L-cysteine (NAC) on the survival of SESN2 KO HepG2 cells under PA stimulation. We observed that GSK'872 partially rescued the decreased cell viability caused by SESN2 knockout. Moreover, the protective effect of GSK'872 on cell survival was comparable to that of NAC but more pronounced than that of Z-VAD-fmk and ferrostatin-1 (Figure 4C). These research findings suggested that SESN2 could protect hepatocytes from lipotoxicity-induced cell death by regulating necroptosis.

SESN2, with its multifaceted modulatory effects, served as a pivotal regulator of hepatocyte homeostasis and exerted protective functions in the development of MASH [16,17]. In this study, we observed that the depletion of SESN2 exacerbated PA-induced lipid accumulation, inflammatory response, oxidative stress, and ER stress. As shown in Figure 4D—H and Supplementary Figs. 4F—J, the depletion of SESN2 exacerbated PA-induced lipid synthesis markers (e.g., SREBP1 and SCD1), MAPK pathway components (e.g., p-P38, p-ERK, and p-JNK), pro-inflammatory cytokines (e.g., TNF-α and IL-1β), and oxidative stress indicators (e.g., ROS and lipid peroxidation). Furthermore, we utilized the RIPK3-specific necroptosis inhibitor, GSK'872, to pharmacologically intervene in SESN2 WT and KO HepG2 cells subjected to PA exposure. Our findings demonstrated that treatment with GSK'872 effectively diminished the expression of SESN2 induced by PA (Figure 4I, Supplementary Fig. 5E), indicating that necroptosis may contribute to the upregulation of SESN2 in the lipotoxicity model. More importantly, our findings demonstrated that treatment with GSK'872 effectively reduced the elevated levels of MAPK pathway components (Figure 4I, Supplementary Figs. 5A—D), pro-inflammatory cytokines (Figure 4J—K), and oxidative stress indicators (Figure 4L-M, Supplementary Fig. 5F) in PA-treated SESN2 KO HepG2 cells. However, GSK'872 treatment did not reverse the dysregulated lipid synthesis and deposition in PA-treated SESN2 KO HepG2 cells (Supplementary Figs. 5J—K).

More than that, we conducted a comparative analysis to assess the effects of RIPK3 inhibitor (GSK'872) and MLKL inhibitor (MLKL—IN—6) on cell death, ROS generation, and IL-1β production induced by PA in both SESN2 WT and KO cells. Firstly, we observed that neither of these inhibitors exhibited complete reversal of the cell death, IL-1β, and ROS induced by PA in both SESN2 WT and KO cells (Supplementary Figs. 5G—I). Moreover, we found that GSK'872 exhibited a relatively weaker suppression of cell death compared to MLKL—IN—6 in PA-treated SESN2 KO cells (Supplementary Fig. 5G). Nevertheless, GSK'872 surpassed MLKL—IN—6 in its efficacy to suppress ROS levels and IL-1β generation in PA-treated SESN2 KO cells (Supplementary Figs. 5H—I). Although the effects mediated by GSK'872 or MLKL—IN—6 were not comprehensive, they adequately demonstrate that the

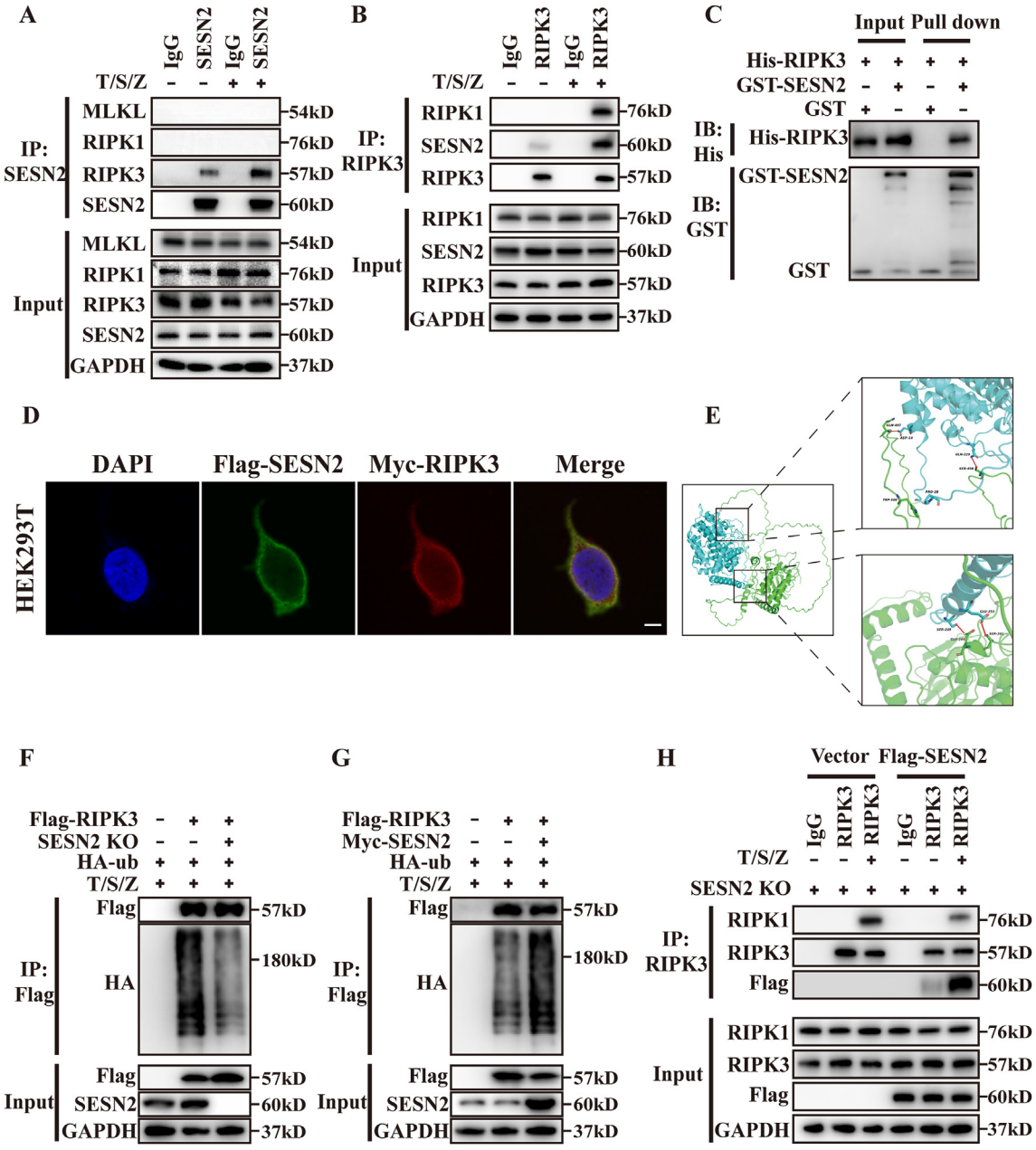

Figure 3: SESN2 interacted with RIPK3 and negatively regulates RIPK1—RIPK3 interaction. (A—B) HepG2 cells lysed and subsequently subjected to immunoprecipitation with specific antibodies against (A) SESN2 or (B) RIPK3 at 1h after exposure to T/S/Z, followed by immunoblotting analysis as indicated. (C) Glutathione S-transferase (GST) pull-down assays showed that the recombinant GST-tagged SESN2 protein exhibited interaction with the His-tagged RIPK3 protein, while no interaction was observed between GST and His-tagged RIPK3. (D) Confocal immunofluorescence images showed that the Flag-SESN2 and Myc-RIPK3 proteins were colocalized in HEK293T cells after exposure to T/S/Z for 1h; Scale bar indicates 10 μm. (E) AlphaFold2-predicted structure of the SESN2 (cyan) bound to RIPK3 (green) shown in two orientations. (F) SESN2 knockout reduced RIPK3 ubiquitination in HepG2 cells. Under T/S/Z stimulation, SESN2 WT and KO HepG2 cells expressed HA-ub and Flag-RIPK3 as indicated. (G) SESN2 overexpression increased RIPK3 ubiquitination in HepG2 cells. Under T/S/Z stimulation, SESN2 WT HepG2 cells expressed HA-ub, Flag-RIPK3, and Myc-SESN2 as indicated. (H) SESN2 KO HepG2 cells were transfected with the Flag-SESN2 vector to express SESN2 in SESN2 KO HepG2 cells. After that, HepG2 cells were treated with T/S/Z for 1h, and the effect of SESN2 induction on RIPK1—RIPK3 complex formation was examined by coimmunoprecipitation. Experiments were repeated at least three times independently, with similar results.

hyperinflammation and excessive oxidative stress observed in SESN2 knockout cells can be partially attributed to the hyperactivation of RIPK3-mediated necroptosis.

On the other hand, we also overexpressed SESN2 in HepG2 cells and conducted a series of experiments to further demonstrate the association between SESN2 and necroptosis. Firstly, we found that the overexpression of SESN2 could ameliorate PA-induced cell death and GSK'872 treatment did not further reduce the cell death in SESN2 overexpression HepG2 cells (Supplementary Figs. 6A and G). Secondly, the overexpression of SESN2 led to reduced phosphorylation levels of RIPK1, RIPK3, and MLKL following PA treatment (Supplementary Fig. 6B). Thirdly, HepG2 cells overexpressing SESN2 exhibited increased level of ubiquitinated RIPK3 following PA treatment (Supplementary Fig. 6C). These results suggested that overexpression

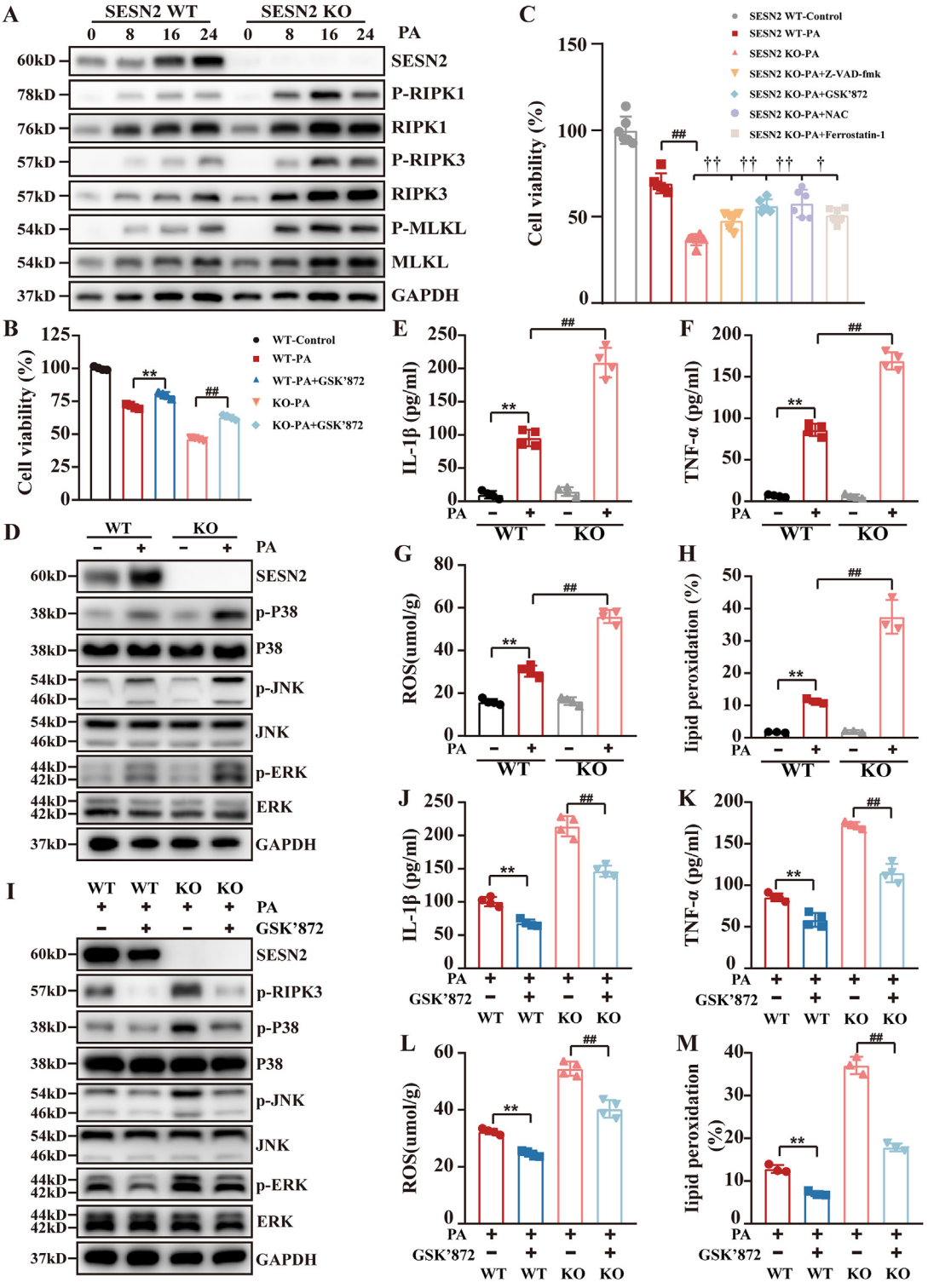

Figure 4: SESN2 protected against palmitic acid (PA)-induced inflammation and oxidative stress partially by inhibiting necroptosis. (A) Western blot analysis of p-RIPK1, RIPK1, p-RIPK3, RIPK3, p-MLKL, MLKL and SESN2 over time in SESN2 WT and SESN2 KO HepG2 cells treated with PA (250 μM) for 24h. (B) CCK8 assay of SESN2 WT and KO HepG2 cells in the present or absence of 5 μM GSK'872 for 24 h. (C) CCK8 assay of SESN2 KO HepG2 cells treated with 250 μM PA in the present or absence of 20 μM Z-VAD-fmk, 5 μM ferrostatin-1, 5 μM GSK'872, 5 mM N-acetyl-L-cysteine (NAC), or DMSO for 24 h. (D) Western blot analysis of SESN2, p-P38, P38, p-JUK, JUK, p-ERK, and ERK in SESN2 WT and SESN2 KO HepG2 cells. (E, J) The level of IL-1β in SESN2 WT and KO HepG2 cells was measured in cell culture supernatant by a commercial ELISA kit. (F, K) (E, J) The level of TNF-α in SESN2 WT and KO HepG2 cells was measured in cell culture supernatant by a commercial ELISA kit. (G, L) The contents of ROS in SESN2 WT and KO HepG2 cells was detected with *in vitro* ROS/reactive nitrogen species assay kit. (H, M) The lipid peroxidation assessment was determined by C11-BODIPY 581/591 and flow cytometry in SESN2 WT and KO HepG2 cells at 6h after exposure to 400 μM PA. The percentage of lipid peroxidation in each group. All the data are expressed as the mean ± SD ($n = 3–5$). *$p < 0.05$, **$p < 0.01$ for SESN2 WT vs SESN2 WT-PA, and SESN2 WT-PA vs SESN2 WT-PA + GSK'872; #$p < 0.05$, ##$p < 0.01$ for SESN2 WT-PA vs SESN2 KO-PA, and SESN2 KO-PA vs SESN2 KO-PA + GSK'872; †$P < 0.05$, ††$P < 0.01$ for SESN2 KO-PA vs SESN2 KO-PA with different inhibitors.

of SESN2 equipped HepG2 cells with the ability to tune down necroptosis by inhibiting the phosphorylation of RIPK3, promoting the ubiquitination of RIPK3 in PA-induced lipotoxicity model.

Finally, we assessed the impact of SESN2 overexpression on PA-induced inflammation and oxidative stress. Here, we found that SESN2 overexpression could significantly reduce the levels of IL-1β, TNF-α and ROS in PA-treated HepG2 cells (Supplementary Figs. 6D—F). More importantly, we demonstrated that the overexpression of SESN2 exhibited a superior impact on the reduction of TNF-α and ROS compared to GSK'872 treatment (Figure 6H—I). Moreover, GSK'872 treatment did not further reduce the levels of TNF-α and ROS in SESN2 overexpression HepG2 cells (Figure 6H—I). Collectively, these results suggested that the overexpression of SESN2 could inhibit PA-induced necroptosis, potentially serving as a mechanism through which SESN2 modulates inflammation and oxidative stress during MASH development.

3.5. SESN2 played an important role in preventing the progression from simple steatosis to MASH partially via suppressing RIPK3-mediated necroptosis in HFHCD-induced MASH mouse model

In our *in vitro* study, we observed an upregulation of SESN2 expression in response to PA, indicating its involvement in the inhibition of necroptosis. In this study, we investigated the expression of SESN2 in paraffin liver sections obtained from patients diagnosed with MASH and individuals serving as normal controls. Immunohistochemistry was employed to assess SESN2 expression, and our findings revealed a significant increase in SESN2 expression within MASH livers when compared to the normal control group (Supplementary Fig. 7A). The finding was consistent with the data from the mouse MASH model, further supporting the crucial role of SESN2 in the progression of MASLD.

To elucidate the role of SESN2 in modulating necroptosis during the progression of MASLD, we initially utilized the GEO dataset GSE167523 [www.ncbi.nlm.nih.gov/gds] to investigate this relationship. Our analysis revealed that the mRNA levels of SESN2, as well as the hallmarks of necroptosis (RIPK1/RIPK3/MLKL), were significantly upregulated in the liver tissues of MASH patients compared to patients with simple steatosis (Supplementary Figs. 7B—E). Furthermore, the correlational analysis revealed that hepatic SESN2 mRNA expression in patients with simple steatosis was positively correlated with the levels of RIPK1 [Pearson's rank correlation coefficient, $R = 0.6450$, $p < 0.0001$], RIPK3 [$R = 0.3442$, $p < 0.05$] and MLKL [$R = 0.3971$, $p < 0.005$] (Supplementary Figs. 7F—H). Moreover, hepatic SESN2 mRNA expression in MASH patients was also positively correlated with the levels of RIPK1 [$R = 0.4518$, $p < 0.005$] (Supplementary Fig. 7I). These data suggested that there might exist connections between SESN2 and necroptosis during MASLD progression.

Our *in vitro* studies have demonstrated that SESN2 could mitigate hepatocyte injury induced by PA through the modulation of RIPK3-mediated necroptosis. Moreover, we isolated primary hepatocytes from the livers of both SESN2 WT and KO mice and utilized Agarose-TUBEs to enrich endogenous polyubiquitin chains in PA-treated primary hepatocytes, followed by immunoblotting for RIPK3. Our results showed that the knockout of SESN2 in mice led to diminished level of ubiquitinated RIPK3 in primary hepatocytes under PA stimulation, which further suggested SESN2 might involve in the regulation of RIPK3-mediated necroptosis during MASH development (Supplementary Fig. 7J). To further investigate the contribution of dysregulated necroptosis in SESN2 KO mice to MASLD development, we employed the RIPK3-specific inhibitor, GSK'872, to treat HFHCD-induced MASH mice (Figure 5A). SESN2 WT and KO mice fed with chow diet exhibited normal histological structure and architecture of liver (Figure 5F). However, 16 weeks of the HFHCD-diet induced significant steatosis, inflammation and hepatocellular ballooning in both WT and KO mice (Supplementary Figs. 8A—D), suggesting that successful establishment of the MASH mouse model, as reported in previous studies [22,23]. Compared to SESN2 WT-HFHCD mice, SESN2 KO-HFHCD mice exhibited elevated levels of RIPK3 and MLKL phosphorylation, along with increased serum alanine aminotransferase (ALT), aspartate aminotransferase (AST), and alkaline phosphatase (ALP) levels (Figure 5B—E, Supplementary Figs. 8F—I). Significantly, the administration of GSK'872 demonstrated a notable reduction in the phosphorylation of RIPK3/MLKL and improvement in liver damage indicators in SESN2-KO HFHCD mice (Figure 5B—E, Supplementary Figs. 8F—I). This finding suggested that SESN2 served as a regulatory element in the progression of MASH, partially by inhibiting RIPK3-mediated necroptosis.

However, consistent with our *in vitro* findings, we observed that GSK'872 treatment did not reverse the increased lipid metabolism abnormalities and hepatic steatosis in SESN2-KO HFHCD mice. Specifically, we observed significant elevations in body weight, liver index, epididymal fat index, serum triglyceride (TG), and total cholesterol (TC) levels in SESN2 KO-HFHCD mice compared to WT-HFHCD mice (Supplementary Figs. 9C—G). However, treatment with GSK'872 failed to improve these indicators in SESN2 KO-HFHCD mice, except for TC (Supplementary Figs. 9C—G). Additionally, there was no significant difference in hepatic steatosis, as observed in HE staining and Oil Red O staining, between SESN2 KO-HFHCD mice and SESN2 KO-HFHCD + GSK'872 mice (Figure 5F, Supplementary Figs. 9A—B). Therefore, we argued that dysregulation of RIPK3-mediated necroptosis was not the primary cause of aggravated lipid metabolism disorders in SESN2 KO mice during the development of MASLD.

The elucidation of mechanisms driving the transition from simple steatosis to MASH is a crucial area of investigation in understanding the pathogenesis of MASLD. This line of research holds significant clinical relevance as simple steatosis is generally considered to have a benign course. However, the presence of MASH-related inflammation, oxidative stress, and hepatocyte death serves as critical driving forces in the progression of MASLD towards fibrosis and even cirrhosis [40—42]. Interestingly, although there were no significant differences in hepatic steatosis between SESN2 KO-HFHCD mice with or without GSK'872 treatment, we observed a notable reduction in the inflammatory score, hepatocyte ballooning, and overall MASLD activity score in SESN2 KO-HFHCD mice after GSK'872 treatment in HE staining (Supplementary Figs. 8B—D). Moreover, SESN2 KO-HFHCD mice exhibited elevated levels of pro-inflammatory cytokines (TNF-α, IL-1β, and IL-6) and increased infiltration of inflammatory cells (F4/80+: macrophages and Ly6g+: neutrophils) compared to WT-HFHCD mice (Figure 6A—G). GSK'872 treatment effectively suppressed pro-inflammatory cytokine expression and inflammatory cell infiltration in SESN2 KO-HFHCD mice (Figure 6A—G). Furthermore, the detrimental effects of SESN2 knockout on the indicators of oxidative damage (e.g., malondialdehyde (MDA), ROS, and glutathione (GSH)) in HFHCD mice were dramatically ameliorated by GSK'872 treatment (Figure 6H—J), suggesting that the inhibition of RIPK3-mediated necroptosis might be one of the mechanisms through which SESN2 maintained hepatic immune homeostasis and redox balance during the progression of MASLD.

Fibrosis serves as a crucial parameter for evaluating the progression of MASH. Therefore, in this study, we first employed Sirius red staining to assess collagen deposition and thus to determine the extent of liver fibrosis in each group of mice. The results of Sirius red staining

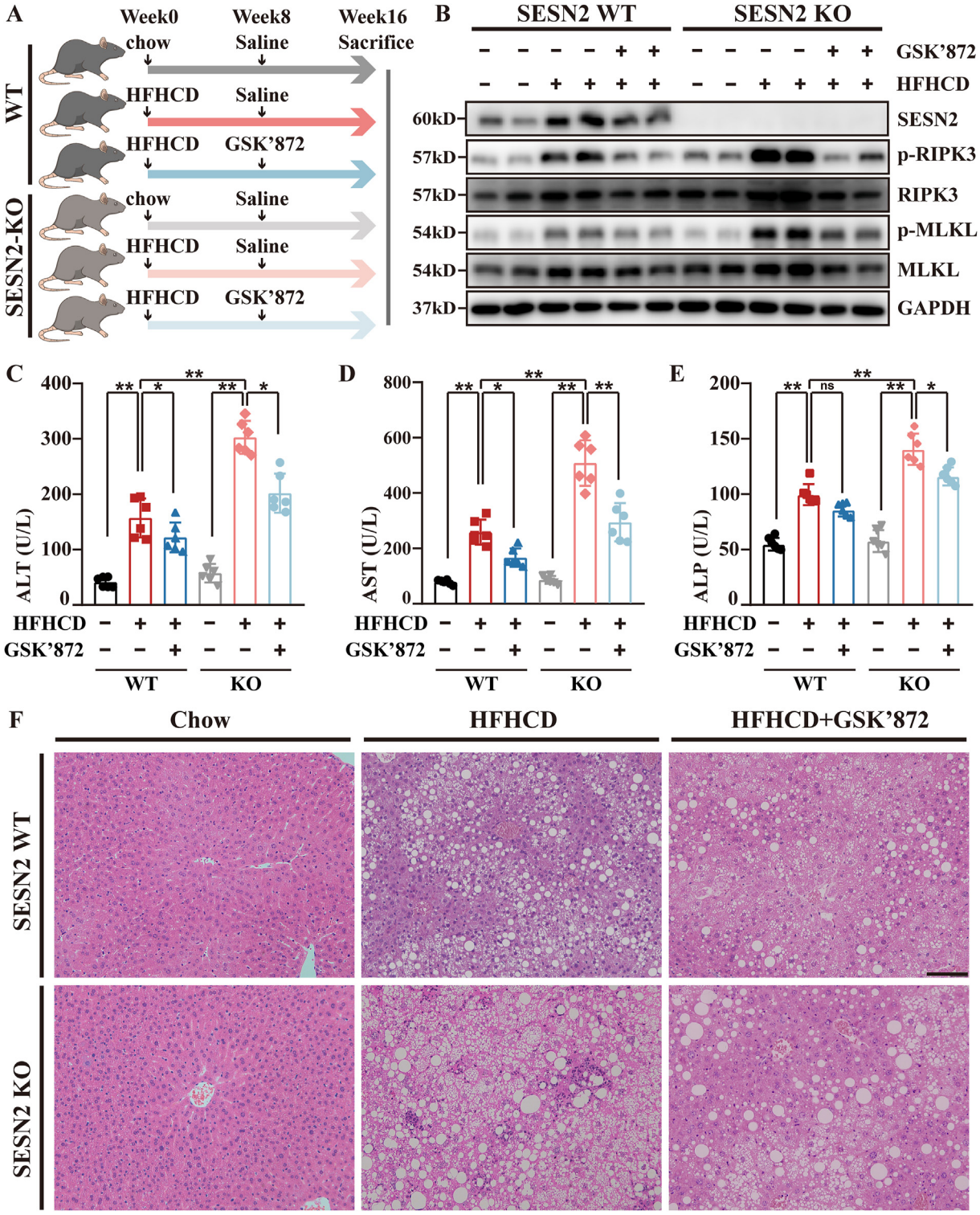

Figure 5: SESN2 acted as a 'brake' in metabolic dysfunction-associated steatohepatitis (MASH) progression partially via suppressing RIPK3-mediated necroptosis. (A) Schematic illustration showing the design of the experimental animal was shown. Eight-week-old male SESN2 WT and SESN2 KO mice were fed with a fed a standard chow diet or a high-fat high-cholesterol diet (HFHCD) for 8 weeks, and then administered intraperitoneally with either the vehicle control or GSK'872 (1 mg/kg) twice weekly for the next 8 weeks. (B) The expression of the indicated proteins (SESN2, p-RIPK3, RIPK3, p-MLKL, MLKL, and GAPDH) in different groups. (C–E) Serum levels of alanine aminotransferase (ALT), aspartate aminotransferase (AST), and alkaline phosphatase (ALP) were detected in each group. (F) Representative hematoxylin and eosin (HE) of the liver sections are shown in each group (scale bar = 100 μm). All the data are expressed as the mean ± SD (n = 6). Statistical analysis was performed by one-way one-way analysis of variance (ANOVA), followed by Tukey's post hoc test for multiple comparisons; *P < 0.05, **P < 0.01.

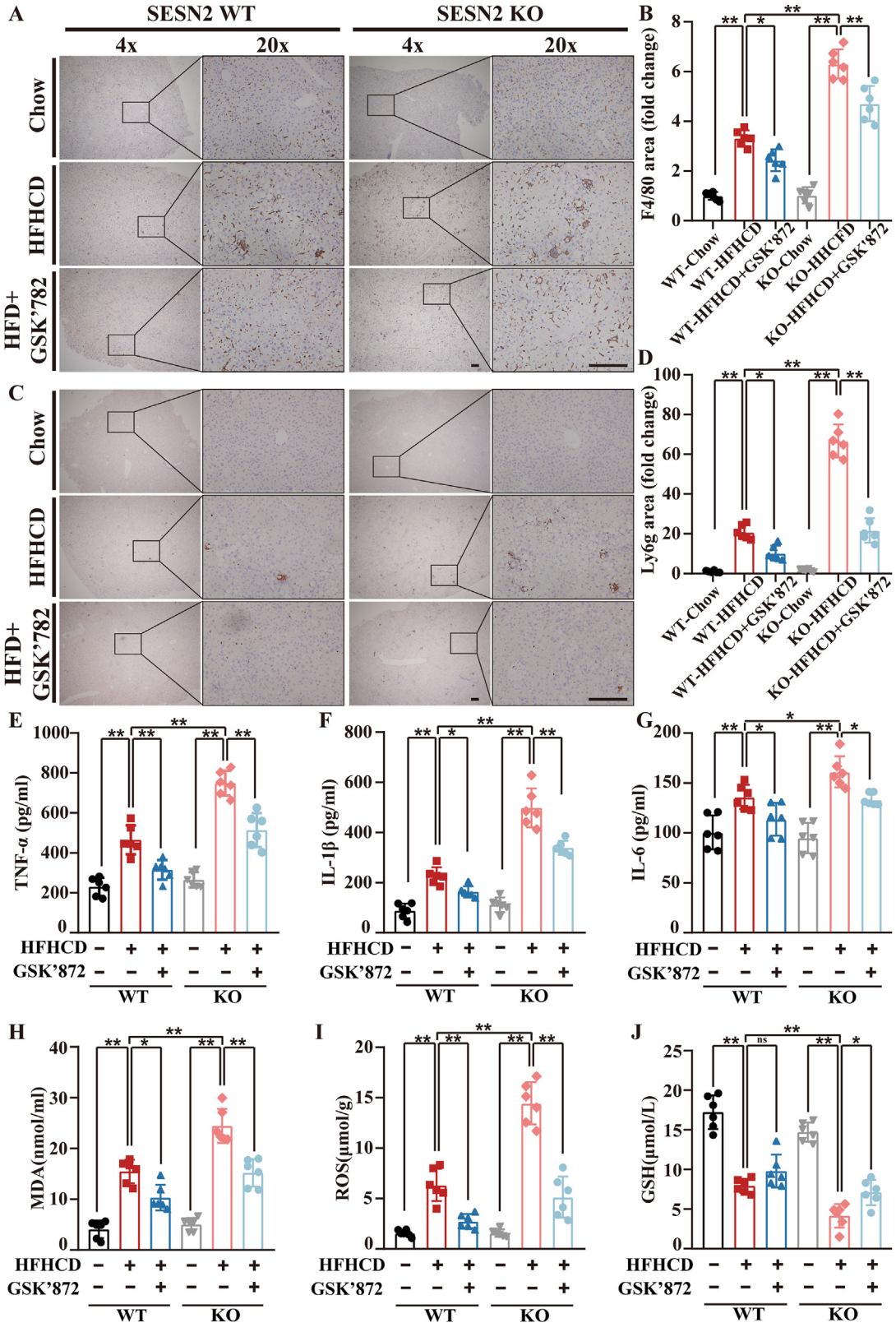

Figure 6: SESN2 suppressed HFHCD-induced inflammation and oxidative stress partially by inhibiting RIPK3-mediated necroptosis. (A, C) Representative immunohistochemical staining of the liver sections showing the expression of (A) F4/80 and (C) Ly6G in each group (scale bar = 200 μm). (B, D) Quantification of F4/80 and Ly6G positive areas in each group. The areas of F4/80/Ly6G-positive cells were evaluated in six randomly selected fields captured at the same magnification. (E–G) The level of serum pro-inflammatory cytokines (TNF-α, IL-1β and IL-6) in each group were assessed by Elisa. (H–J) Hepatic malondialdehyde (MDA), ROS and glutathione (GSH) were assessed in each group. All the data are expressed as the mean ± SD (n = 6). Statistical analysis was performed by one-way ANOVA, followed by Tukey's post hoc test for multiple comparisons; $^{*}P < 0.05$, $^{**}P < 0.01$.

showed that SESN2 knockout exacerbated HFHCD-induced hepatic collagen deposition (Figure 7A—B). In contrast, GSK'872 treatment demonstrated significant efficacy in reducing hepatic collagen deposition, particularly within the intralobular region in SESN2 KO-HFHCD mice (Figure 7A—B). Under pathological circumstances, quiescent HSC could differentiate into fibrotic cells, characterized by the expression of α-SMA and collagen type I [43,44]. Consequently, we next utilized the HSC activation marker (α-SMA and collagen type I alpha 1 chain (COL1A1)) to indirectly evaluate the potential involvement of dysregulated necroptosis in the progression of hepatic fibrosis in SESN2 KO mice. According to immunohistochemistry analysis of α-SMA and COL1A1, we found that SESN2 knockout significantly exacerbated HFHCD-induced HSC activation, which was subsequently ameliorated following treatment with GSK'872 (Figure 7C—F). However, it should be noted that a 16-week HFHCD diet is insufficient to induce a significant hepatic fibrosis phenotype. Therefore, more liver fibrosis models are needed to further verify these conclusions.

4. DISCUSSION

Indeed, our findings unveiled a novel mechanism by which SESN2 was activated under necroptosis-inducing conditions and functioned as a negative regulator of necroptosis. Elevated SESN2 inhibited RIPK3 phosphorylation, enhanced RIPK3 ubiquitination, and prevented RIPK1/RIPK3 necrosome activation; this regulation might be one of the mechanisms through which SESN2 mediates anti-inflammatory and anti-oxidative stress responses during MASLD development (Figure 8). To date, the mechanisms underlying the negative regulation of necroptosis were only partially understood [35]. Notably, in addition to previously identified negative regulators of necroptosis, such as Parkin [35], Ppm1b [45], and AURKA [46], our present study offered a novel insight in this aspect. In this study, we observed that SESN2 is activated in a time-dependent manner under T/S/Z-induced necroptotic conditions, suggesting a potential link between necroptosis and SESN2 activation. One possible explanation for this was that the release of DAMPs from necroptotic cells could serve as signaling molecules that effectively activate SESN2 expression [13,14,16,17,20]. However, what role might activate SESN2 play in the necroptotic process? Here, we identified that SESN2 served as a negative regulator of necroptosis and inhibited inflammation and oxidative stress in T/S/Z-induced necroptosis model. It's important to note that although T/S/Z was a specific model for inducing necroptosis, SESN2 knockdown-related alterations in this model might not be exclusively attributed to necroptosis. This is because T/S/Z not only elicits inflammation and oxidative stress via the release of DAMPs following necroptosis, but also triggers inflammation and oxidative stress through the activation of other mechanisms, such as the TNFR signaling. Therefore, this raised a question: In the T/S/Z model, did SESN2 block inflammation, oxidative stress, and necroptosis collectively, or did SESN2 block utilized the necroptosis inhibitor GSK'872 for validation. Our results showed GSK'872 treatment could significantly reduce the levels of IL-1β and ROS in T/S/Z-treated KO cells, although this effect was not complete. Therefore, these results suggested SESN2 mitigated inflammation and oxidative stress, at least in part, through its regulation of necroptosis activation in T/S/Z-induced necroptosis model.

To further elucidate the molecular mechanisms, verification of the molecules interacting with SESN2 is necessary. Here, we found that SESN2 coimmunoprecipitated with RIPK3, but not with MLKL or RIPK1, and served as a suppressor in inhibiting the assembly of the necrosome complex (RIPK1-RIPK3). To determine how SESN2 regulate RIPK3-mediated necroptosis, we investigated post-translational modifications of RIPK3, which have been identified as important for the activation of necroptosis [11,34]. Our findings indicated that SESN2 played a crucial role in the regulation of necroptosis by inhibiting the phosphorylation of RIPK3 and facilitating its ubiquitination, thereby effectively preventing RIPK3-mediated necroptosis. It has been reported that RIPK3 activation leads to the generation of ROS [31]. Moreover, the formation of RIPK1/RIPK3 necrosomes is accompanied by inflammation [47]. Therefore, we further hypothesized that in T/S/Z-induced necroptosis model, SESN2 was involved in the regulation of inflammation and oxidative stress, not only by reducing the release of DAMPs after necroptosis, but also by influencing the activation process of necroptosis, such as inhibiting RIPK3 and decreasing the assembly of necrosome. However, it should be noted that SESN2 protein itself lacks the characteristic motif of an E3 ubiquitin ligase, suggesting that SESN2 did not directly induce the ubiquitination of RIPK3. Instead, SESN2 may act as a platform or adaptor, facilitating the recognition and binding of downstream E3 ligases to RIPK3, thereby indirectly mediating the ubiquitination process. Therefore, it will be interesting to elucidate how the ubiquitination modification of RIPK3 is regulated by SESN2 in greater detail in future studies.

Hepatocyte death is a critical event in the progression of liver diseases, and the occurrence of substantial hepatocyte death is a key distinction between steatohepatitis and simple steatosis [48]. Long-term chronic hepatocyte death triggers persistent hepatocyte proliferation, immune cell recruitment, and activation of hepatic stellate cells, ultimately driving the development of MASLD towards liver fibrosis and cirrhosis [10]. As yet, accumulating evidence has substantiated the crucial involvement of SESN2 in maintaining hepatocyte survival and limiting MASH progression, which is emerging as a key target for MASH therapy [17]. Nonetheless, our comprehension of the underlying mechanisms responsible for the protective effects of SESN2 remains incomplete. Traditionally, apoptosis has been widely regarded as the primary mechanism through which SESN2 modulates hepatocyte survival [49]. However, it has become evident that this perspective oversimplifies the intricate landscape of SESN2's functions. In this study, we unveiled a novel function of SESN2 in regulating hepatocyte necroptosis during MASLD development, providing multiple lines of evidence to support this notion. Firstly, knockdown of SESN2 led to a significant increase in PA-induced cell death, accompanied by enhanced phosphorylation of necroptotic kinases.

Secondly, we examined the impact of the necroptosis inhibitor GSK'872 on the viability of SESN2 KO cells. Our findings revealed a significant mitigation of PA-induced cell death in SESN2 KO cells by GSK'872, further suggesting the involvement of necroptosis in the heightened cell death in SESN2 KO cells. Thirdly, we examined the impact of the necroptosis inhibitor GSK'872, as well as other inhibitors targeting different types of cell death (such as Z-VAD-fmk, ferrostatin-1, and NAC), on the survival of SESN2 KO cells under PA stimulation. Our results indicated that, in addition to other forms of cell death, necroptosis represented a significant component of the cell death response induced by SESN2 knockout in the PA-induced lipotoxicity model. However, it should be noted that despite the observed upregulation of SESN2 in pathological circumstances, its level of expression remained inadequate in attenuating the advancement of MASH. Consequently, we proceeded to overexpress SESN2 in HepG2 cells as a means of substantiating our findings. Here, we found that overexpression of SESN2 could equip HepG2 cells with the ability to tune down necroptosis by inhibiting the phosphorylation of RIPK3, promoting the ubiquitination of RIPK3 in PA-induced *in vitro* MASH model. In summary, compelling evidence from

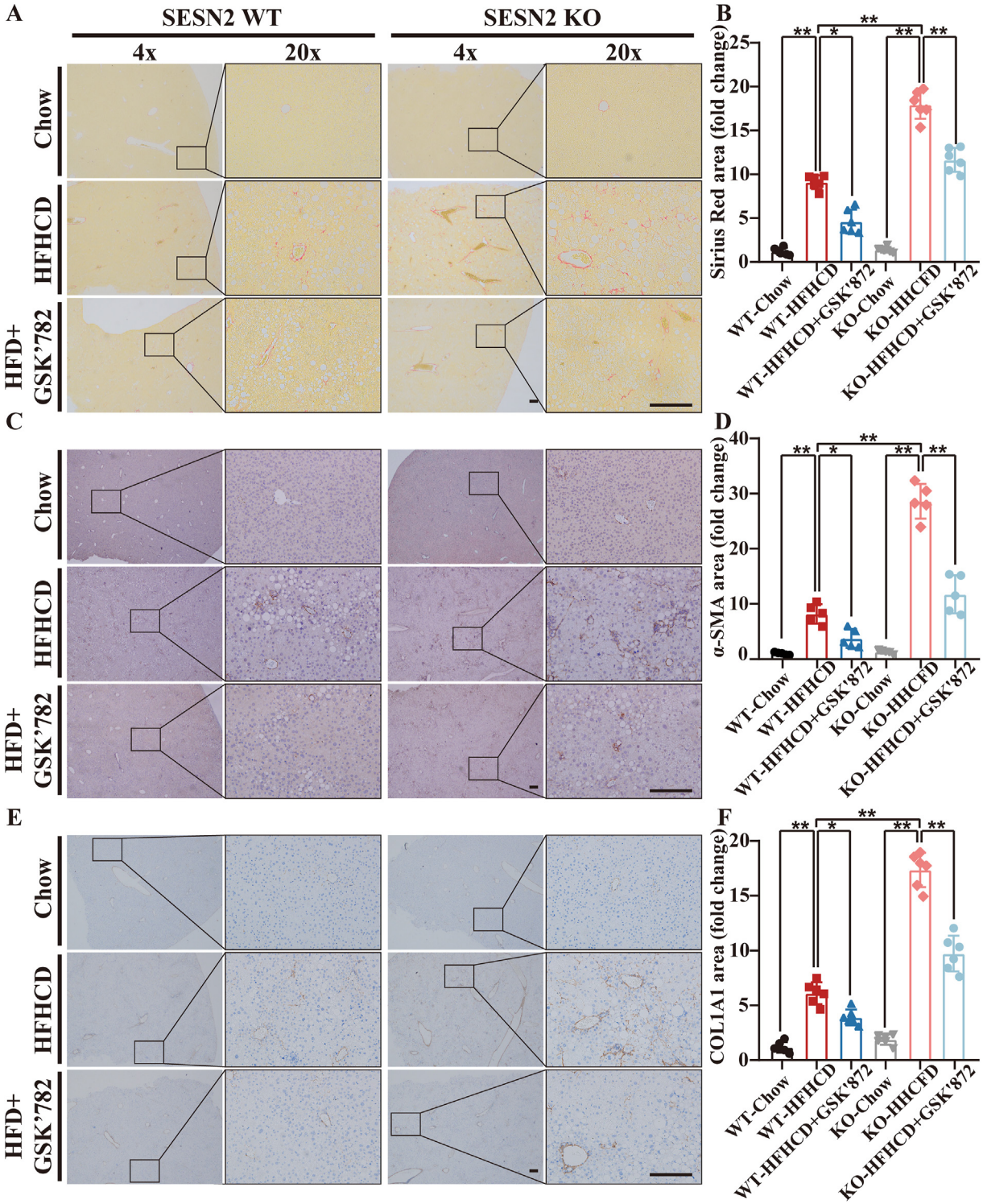

Figure 7: SESN2 suppressed HFHCD-induced fibrosis partially by inhibiting RIPK3-mediated necroptosis. (A) Representative Sirius red staining of the liver sections is shown in each group (scale bar = 200 μm). (B) Quantification of in each group. The areas of collagen deposition detected by Sirius red were evaluated in five randomly selected fields captured at the same magnification. (C, E) Representative immunohistochemical staining of the liver sections showing the expression of (C) α-SMA and (E) collagen type I alpha 1 chain (COL1A1) in each group (scale bar = 200 μm). (D, F) Quantification of α-SMA and COL1A1 in each group. The areas of α-SMA-positive cells were evaluated in five randomly selected fields captured at the same magnification. (n = 5–6). Statistical analysis was performed by one-way ANOVA, followed by Tukey's post hoc test for multiple comparisons; *P < 0.05, **P < 0.01.

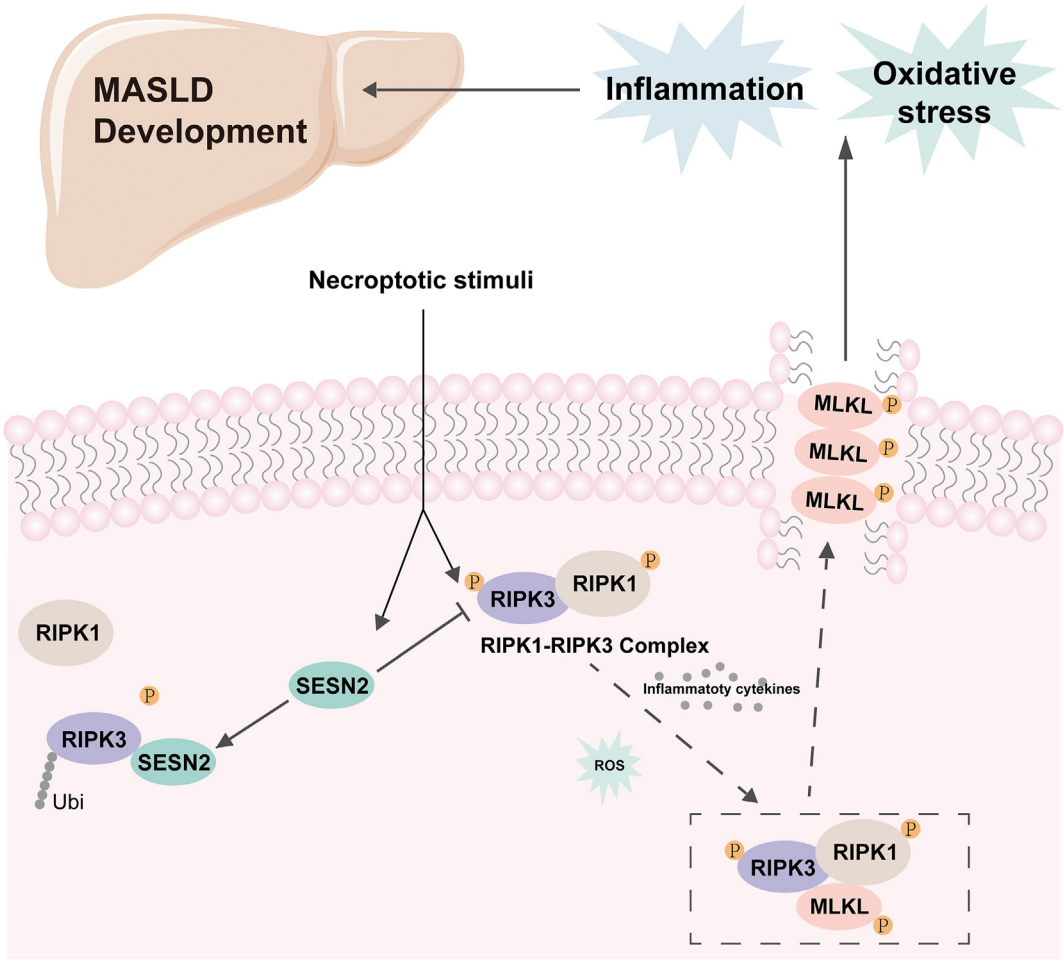

Figure 8: A schematic model of how the SESN2 negatively modulates necroptosis during MASLD development. SESN2 is activated under necroptosis-inducing conditions and functions as a negative regulator of necroptosis. Elevated SESN2 inhibit RIPK3 phosphorylation, enhance RIPK3 ubiquitination, and prevent necrosome activation and subsequent MLKL-mediated membrane destruction; this regulation might be one of the mechanisms through which SESN2 mediates anti-inflammatory and anti-oxidative stress responses during metabolic dysfunction-associated steatotic liver disease (MASLD) development.

our study, as well as previous research [38,39], strongly supported the critical role of SESN2 in regulating hepatocyte death and survival, thus restraining the progression of MASH.

Considering the multifunctional role of SESN2 [17,18], we wanted to elucidate whether the regulation of SESN2 on necroptosis is important for MASH progression. To identify the phenotypes of MASH in SESN2 KO mice attributed to RIPK3-mediated necroptosis, we utilized GSK'872, a RIPK3-specific necroptosis inhibitor, to treat mice. Consistent with our *in vitro* findings, GSK'872 treatment effectively suppressed the expression of pro-inflammatory cytokines, infiltration of inflammatory cells, and oxidative damage in SESN2 KO-HFHCD mice. Moreover, GSK'872 treatment led to a reduction in initial indicators of fibrosis in SESN2 KO-HFHCD mice. These results suggested that SESN2 played a crucial role in maintaining hepatic immune homeostasis and redox balance partially by inhibiting RIPK3-mediated necroptosis during MASLD development, ultimately impeding the progression of MASH to fibrosis and cirrhosis. Interestingly, it has been reported that RIPK3 acts as a regulator of lipid metabolism in MASLD progression [50,51]. Moreover, the GEO dataset revealed a positive correlation between the levels of SESN2 and RIPK3 at the simple steatosis stage, but not the MASH stage. However, our studies observed that inhibition of RIPK3 by GSK'872 was not able to reverse the increased lipid metabolism abnormalities and steatosis in SESN2-KO HFHCD mice. How can we explain these seemingly contradictory results? We proposed that the suppression of RIPK3 by SESN2 was primarily regulated at the translation and post-translational modification levels, rather than at the transcriptional level. Furthermore, the function of SESN2 in regulating hepatic lipid metabolism might be independent of RIPK3-mediated necroptosis, and SESN2 may exert this function by modulating other mechanisms. For example, SESN2 could reduce lipid synthesis and enhance the clearance of lipid droplet by activating AMPK and inhibiting mTOR1 [52,53]. Moreover, SESN2 could regulate mitochondrial biogenesis and lipid β-oxidation within hepatocytes, thereby ameliorating hepatic lipid deposition [54].

This study has the following points worthy of further improvement. Firstly, the E3 ubiquitin ligases that catalyze RIPK3 ubiquitination were not known. Another limitation in our study is the lack of hepatocyte-specific SESN2 knockout and hepatocyte-specific SESN2 overexpression mice. The exact role of SESN2 in necroptosis during MASLD development could be better clarified if hepatocyte-specific SESN2 knockout or overexpression mice were used in the future. Third, although this study was validated using HepG2 cells, further studies are needed to validate in primary hepatocytes or AML12 cells.

In conclusion, this study has uncovered a novel molecular function of SESN2 as a negative regulator of necroptosis, with physiological significance in restraining RIPK3 activation in the pathogenesis of MASH. Our findings also highlight the importance of the SESN2/RIPK3 axis in maintaining hepatic immune homeostasis and redox balance, thereby providing potential therapeutic targets for the treatment of human MASH in the future.

FUNDING

This work was financially supported by grants from the National Natural Science Foundation of China (No: 82170593) to Jian-Gao Fan.

CREDIT AUTHORSHIP CONTRIBUTION STATEMENT

Jian-Bin Zhang: Writing — original draft, Methodology, Investigation, Conceptualization. **Qian-Ren Zhang:** Writing — original draft, Methodology, Investigation. **Qian Jin:** Methodology, Investigation. **Jing Yang:** Methodology, Investigation. **Shuang-Zhe Lin:** Methodology. **Jian-Gao Fan:** Writing — review & editing, Funding acquisition, Data curation, Conceptualization.

ACKNOWLEDGEMENTS

We thank Dr. Wenning Xu for SESN2 knockout (SESN2 KO) C57BL/6 mice, as well as Dr. Wanqun Xie for pLVML vector, pGEX-4T-1 vector, pET-28a vector and insightful discussion.

DECLARATION OF COMPETING INTEREST

The authors declare that they have no known competing financial interests or personal relationships that could have appeared to influence the work reported in this paper.

DATA AVAILABILITY

Data will be made available on request.

APPENDIX A. SUPPLEMENTARY DATA

Supplementary data to this article can be found online at https://doi.org/10.1016/j.molmet.2023.101865.

REFERENCES

[1] Francque SM, Marchesini G, Kautz A, Walmsley M, Dorner R, Lazarus JV, et al. Non-alcoholic fatty liver disease: a patient guideline. JHEP Rep 2021;3(5):100322. https://doi.org/10.1016/j.jhepr.2021.100322. PMID:34693236.

[2] Haas JT, Francque S, Staels B. Pathophysiology and mechanisms of nonalcoholic fatty liver disease. Annu Rev Physiol 2016;78:181—205. https://doi.org/10.1146/annurev-physiol-021115-105331. PMID:26667070.

[3] Ayonrinde OT. Historical narrative from fatty liver in the nineteenth century to contemporary NAFLD - reconciling the present with the past. JHEP Rep 2021;3(3):100261. https://doi.org/10.1016/j.jhepr.2021.100261. PMID:34036255.

[4] M.E. R, V LJ, V R, Sm F, Aj S, F K. A multi-society delphi consensus statement on new fatty liver disease nomenclature. J Hepatol 2023. https://doi.org/10.1016/j.jhep.2023.06.003.

[5] Yilmaz Y, Toraman AE, Alp C, Doğan Z, Keklikkiran C, Stepanova M, et al. Impairment of patient-reported outcomes among patients with non-alcoholic fatty liver disease: a registry-based study. Aliment Pharmacol Ther 2023;57(2):215—23. https://doi.org/10.1111/apt.17301. PMID:36369643.

[6] Bertheloot D, Latz E, Franklin BS. Necroptosis, pyroptosis and apoptosis: an intricate game of cell death. Cell Mol Immunol 2021;18(5):1106—21. https://doi.org/10.1038/s41423-020-00630-3. PMID:33785842.

[7] Malhi H, Gores GJ, Lemasters JJ. Apoptosis and necrosis in the liver: a tale of two deaths? Hepatology 2006;43(2 Suppl 1):S31—44. https://doi.org/10.1002/hep.21062. PMID:16447272.

[8] Degterev A, Huang Z, Boyce M, Li Y, Jagtap P, Mizushima N, et al. Chemical inhibitor of nonapoptotic cell death with therapeutic potential for ischemic brain injury. Nat Chem Biol 2005;1(2):112—9. https://doi.org/10.1038/nchembio711. PMID:16408008.

[9] Grootjans S, Vanden Berghe T, Vandenabeele P. Initiation and execution mechanisms of necroptosis: an overview. Cell Death Differ 2017;24(7):1184—95. https://doi.org/10.1038/cdd.2017.65. PMID:28498367.

[10] Schwabe RF, Luedde T. Apoptosis and necroptosis in the liver: a matter of life and death. Nat Rev Gastroenterol Hepatol 2018;15(12):738—52. https://doi.org/10.1038/s41575-018-0065-y. PMID:30250076.

[11] Seo J, Nam YW, Kim S, Oh DB, Song J. Necroptosis molecular mechanisms: recent findings regarding novel necroptosis regulators. Exp Mol Med 2021;53(6):1007—17. https://doi.org/10.1038/s12276-021-00634-7. PMID:34075202.

[12] Xu H, Du X, Liu G, Huang S, Du W, Zou S, et al. The pseudokinase MLKL regulates hepatic insulin sensitivity independently of inflammation. Mol Metab 2019;23:14—23. https://doi.org/10.1016/j.molmet.2019.02.003. PMID:30837196.

[13] Kaczmarek A, Vandenabeele P, Krysko DV. Necroptosis: the release of damage-associated molecular patterns and its physiological relevance. Immunity 2013;38(2):209—23. https://doi.org/10.1016/j.immuni.2013.02.003. PMID:23438821.

[14] Weinlich R, Oberst A, Beere HM, Green DR. Necroptosis in development, inflammation and disease. Nat Rev Mol Cell Biol 2017;18(2):127—36. https://doi.org/10.1038/nrm.2016.149. PMID:27999438.

[15] Kubes P, Mehal WZ. Sterile inflammation in the liver. Gastroenterology 2012;143(5):1158—72. https://doi.org/10.1053/j.gastro.2012.09.008. PMID:22982943.

[16] Wang BJ, Wang S, Xiao M, Zhang J, Wang AJ, Guo Y, et al. Regulatory mechanisms of Sesn2 and its role in multi-organ diseases. Pharmacol Res 2021;164:105331. https://doi.org/10.1016/j.phrs.2020.105331. PMID:33285232.

[17] Lu C, Jiang Y, Xu W, Bao X. Sestrin2: multifaceted functions, molecular basis, and its implications in liver diseases. Cell Death Dis 2023;14(2):160. https://doi.org/10.1038/s41419-023-05669-4. PMID:36841824.

[18] Yang JH, Kim KM, Kim MG, Seo KH, Han JY, Ka SO, et al. Role of sestrin2 in the regulation of proinflammatory signaling in macrophages. Free Radic Biol Med 2015;78:156—67. https://doi.org/10.1016/j.freeradbiomed.2014.11.002. PMID:25463278.

[19] Park HW, Park H, Ro SH, Jang I, Semple IA, Kim DN, et al. Hepatoprotective role of Sestrin2 against chronic ER stress. Nat Commun 2014;5:4233. https://doi.org/10.1038/ncomms5233. PMID:24947615.

[20] Pasparakis M, Vandenabeele P. Necroptosis and its role in inflammation. Nature 2015;517(7534):311—20. https://doi.org/10.1038/nature14191. PMID:25592536.

[21] Xu WN, Liu C, Zheng HL, Xu HX, Yang RZ, Jiang SD, et al. Sesn2 serves as a regulator between mitochondrial unfolded protein response and mitophagy in intervertebral disc degeneration. Int J Biol Sci 2023;19(2):571—92. https://doi.org/10.7150/ijbs.70211. PMID:36632468.

[22] Liu XL, Pan Q, Cao HX, Xin FZ, Zhao ZH, Yang RX, et al. Lipotoxic hepatocyte-derived exosomal MicroRNA 192-5p activates macrophages through rictor/akt/forkhead box transcription factor O1 signaling in nonalcoholic fatty liver

disease. Hepatology 2020;72(2):454–69. https://doi.org/10.1002/hep.31050. PMID:31782176.

[23] Zhao ZH, Xin FZ, Xue Y, Hu Z, Han Y, Ma F, et al. Indole-3-propionic acid inhibits gut dysbiosis and endotoxin leakage to attenuate steatohepatitis in rats. Exp Mol Med 2019;51(9):1–14. https://doi.org/10.1038/s12276-019-0304-5. PMID:31506421.

[24] Zhang F, Hu Z, Li G, Huo S, Ma F, Cui A, et al. Hepatic CREBZF couples insulin to lipogenesis by inhibiting insig activity and contributes to hepatic steatosis in diet-induced insulin-resistant mice. Hepatology 2018;68(4):1361–75. https://doi.org/10.1002/hep.29926. PMID:29637572.

[25] Zhou D, Pan Q, Xin FZ, Zhang RN, He CX, Chen GY, et al. Sodium butyrate attenuates high-fat diet-induced steatohepatitis in mice by improving gut microbiota and gastrointestinal barrier. World J Gastroenterol 2017;23(1):60–75. https://doi.org/10.3748/wjg.v23.i1.60. PMID:28104981.

[26] Li Y, Xu S, Mihaylova MM, Zheng B, Hou X, Jiang B, et al. AMPK phosphorylates and inhibits SREBP activity to attenuate hepatic steatosis and atherosclerosis in diet-induced insulin-resistant mice. Cell Metabol 2011;13(4):376–88. https://doi.org/10.1016/j.cmet.2011.03.009. PMID: 21459323.

[27] Zhang J, Jiang D, Lin S, Cheng Y, Pan J, Ding W, et al. Prolyl endopeptidase disruption reduces hepatic inflammation and oxidative stress in methionine-choline-deficient diet-induced steatohepatitis. Life Sci 2021;270:119131. https://doi.org/10.1016/j.lfs.2021.119131. PMID:33516698.

[28] Zurhove K, Nakajima C, Herz J, Bock HH, May P. Gamma-secretase limits the inflammatory response through the processing of LRP1. Sci Signal 2008;1(47): ra15. https://doi.org/10.1126/scisignal.1164263. PMID:19036715.

[29] Yao H, Tang H, Zhang Y, Zhang QF, Liu XY, Liu YT, et al. DEPTOR inhibits cell proliferation and confers sensitivity to dopamine agonist in pituitary adenoma. Cancer Lett 2019;459:135–44. https://doi.org/10.1016/j.canlet.2019.05.043. PMID:31176743.

[30] Zhang T, Zhang Y, Cui M, Jin L, Wang Y, Lv F, et al. CaMKII is a RIP3 substrate mediating ischemia- and oxidative stress-induced myocardial necroptosis. Nat Med 2016;22(2):175–82. https://doi.org/10.1038/nm.4017. PMID:26726877.

[31] Zhang DW, Shao J, Lin J, Zhang N, Lu BJ, Lin SC, et al. RIP3, an energy metabolism regulator that switches TNF-induced cell death from apoptosis to necrosis. Science 2009;325(5938):332–6. https://doi.org/10.1126/science.1172308. PMID:19498109.

[32] Adasme MF, Linnemann KL, Bolz SN, Kaiser F, Salentin S, Haupt VJ, et al. PLIP 2021: expanding the scope of the protein-ligand interaction profiler to DNA and RNA. Nucleic Acids Res 2021;49(W1):W530–4. https://doi.org/10.1093/nar/gkab294. PMID:33950214.

[33] Laskowski RA, Swindells MB. LigPlot+: multiple ligand-protein interaction diagrams for drug discovery. J Chem Inf Model 2011;51(10):2778–86. https://doi.org/10.1021/ci200227u. PMID:21919503.

[34] Meng Y, Sandow JJ, Czabotar PE, Murphy JM. The regulation of necroptosis by post-translational modifications. Cell Death Differ 2021;28(3):861–83. https://doi.org/10.1038/s41418-020-00722-7. PMID:33462412.

[35] Lee SB, Kim JJ, Han SA, Fan Y, Guo LS, Aziz K, et al. The AMPK-Parkin axis negatively regulates necroptosis and tumorigenesis by inhibiting the necrosome. Nat Cell Biol 2019;21(8):940–51. https://doi.org/10.1038/s41556-019-0356-8. PMID:31358971.

[36] Zhou M, He J, Shi Y, Liu X, Luo S, Cheng C, et al. ABIN3 negatively regulates necroptosis-induced intestinal inflammation through recruiting A20 and restricting the ubiquitination of RIPK3 in inflammatory bowel disease. J Crohns Colitis 2021;15(1):99–114. https://doi.org/10.1093/ecco-jcc/jjaa131. PMID: 32599618.

[37] Huang D, Chen P, Huang G, Sun H, Luo X, He C, et al. Salt-inducible kinases inhibitor HG-9-91-01 targets RIPK3 kinase activity to alleviate necroptosis-mediated inflammatory injury. Cell Death Dis 2022;13(2):188. https://doi.org/10.1038/s41419-022-04633-y. PMID:35217652.

[38] Xu D, Liu L, Zhao Y, Yang L, Cheng J, Hua R, et al. Melatonin protects mouse testes from palmitic acid-induced lipotoxicity by attenuating oxidative stress and DNA damage in a SIRT1-dependent manner. J Pineal Res 2020;69(4): e12690. https://doi.org/10.1111/jpi.12690. PMID:32761924.

[39] Magtanong L, Ko PJ, Dixon SJ. Emerging roles for lipids in non-apoptotic cell death. Cell Death Differ 2016;23(7):1099–109. https://doi.org/10.1038/cdd.2016.25. PMID:26967968.

[40] Sutti S, Jindal A, Locatelli I, Vacchiano M, Gigliotti L, Bozzola C, et al. Adaptive immune responses triggered by oxidative stress contribute to hepatic inflammation in NASH. Hepatology 2014;59(3):886–97. https://doi.org/10.1002/hep.26749. PMID:24115128.

[41] Xu R, Huang H, Zhang Z, Wang FS. The role of neutrophils in the development of liver diseases. Cell Mol Immunol 2014;11(3):224–31. https://doi.org/10.1038/cmi.2014.2. PMID:24633014.

[42] Spahis S, Delvin E, Borys JM, Levy E. Oxidative stress as a critical factor in nonalcoholic fatty liver disease pathogenesis. Antioxid Redox Signal 2017;26(10): 519–41. https://doi.org/10.1089/ars.2016.6776. PMID:27452109.

[43] Wu J, Huang J, Kuang S, Chen J, Li X, Chen B, et al. Synergistic MicroRNA therapy in liver fibrotic rat using MRI-visible nanocarrier targeting hepatic stellate cells. Adv Sci 2019;6(5):1801809. https://doi.org/10.1002/advs.201801809. PMID:30886803.

[44] Mormone E, Lu Y, Ge X, Fiel MI, Nieto N. Fibromodulin, an oxidative stress-sensitive proteoglycan, regulates the fibrogenic response to liver injury in mice. Gastroenterology 2012;142(3):612–621.e5. https://doi.org/10.1053/j.gastro.2011.11.029. PMID:22138190.

[45] Chen W, Wu J, Li L, Zhang Z, Ren J, Liang Y, et al. Ppm1b negatively regulates necroptosis through dephosphorylating Rip3. Nat Cell Biol 2015;17(4):434–44. https://doi.org/10.1038/ncb3120. PMID:25751141.

[46] Xie Y, Zhu S, Zhong M, Yang M, Sun X, Liu J, et al. Inhibition of aurora kinase A induces necroptosis in pancreatic carcinoma. Gastroenterology 2017;153(5): 1429–1443.e5. https://doi.org/10.1053/j.gastro.2017.07.036. PMID:28764929.

[47] Wallach D, Kovalenko A, Kang TB. 'Necrosome'-induced inflammation: must cells die for it? Trends Immunol 2011;32(11):505–9. https://doi.org/10.1016/j.it.2011.07.004. PMID:21890409.

[48] Stefan N, Häring HU, Cusi K. Non-alcoholic fatty liver disease: causes, diagnosis, cardiometabolic consequences, and treatment strategies. Lancet Diabetes Endocrinol 2019;7(4):313–24. https://doi.org/10.1016/s2213-8587(18)30154-2. PMID:30174213.

[49] Ala M, Eftekhar SP. Target Sestrin2 to rescue the damaged organ: mechanistic insight into its function. Oxid Med Cell Longev 2021;2021:8790369. https://doi.org/10.1155/2021/8790369. PMID:34765085.

[50] Afonso MB, Rodrigues PM, Mateus-Pinheiro M, Simão AL, Gaspar MM, Majdi A, et al. RIPK3 acts as a lipid metabolism regulator contributing to inflammation and carcinogenesis in non-alcoholic fatty liver disease. Gut 2021;70(12):2359–72. https://doi.org/10.1136/gutjnl-2020-321767. PMID:33361348.

[51] Afonso MB, Islam T, Magusto J, Amorim R, Lenoir V, Simões RF, et al. RIPK3 dampens mitochondrial bioenergetics and lipid droplet dynamics in metabolic liver disease. Hepatology 2023;77(4):1319–34. https://doi.org/10.1002/hep.32756. PMID:36029129.

[52] Kim H, An S, Ro SH, Teixeira F, Park GJ, Kim C, et al. Janus-faced Sestrin2 controls ROS and mTOR signalling through two separate functional domains. Nat Commun 2015;6:10025. https://doi.org/10.1038/ncomms10025. PMID: 26612684.

[53] Saxton RA, Knockenhauer KE, Wolfson RL, Chantranupong L, Pacold ME, Wang T, et al. Structural basis for leucine sensing by the Sestrin2-mTORC1 pathway. Science 2016;351(6268):53–8. https://doi.org/10.1126/science.aad2087. PMID:26586190.

[54] Lee JH, Budanov AV, Talukdar S, Park EJ, Park HL, Park HW, et al. Maintenance of metabolic homeostasis by Sestrin2 and Sestrin3. Cell Metabol 2012;16(3):311–21. https://doi.org/10.1016/j.cmet.2012.08.004. PMID: 22958918.

